Field Measurements of the Amount of Surface Layer Air versus Height in the Entrainment Zone

TIMOTHY D. CRUM* AND ROLAND B. STULL

Boundary Layer Research Team, Department of Meteorology, University of Wisconsin, Madison, WI 53706

(Manuscript received 5 March 1986, in final form 2 April 1987)

ABSTRACT

The structure of the atmospheric entrainment zone, an interfacial layer between the convective boundary layer and the stable air aloft, is studied using coincident high resolution aircraft and lidar observations obtained during Boundary Layer Experiment–1983 in Oklahoma. Humidity as measured by a fast-response Lyman alpha humidiometer is used as a tracer to estimate the amount of surface-layer origin air reaching various heights in the entrainment zone.

Two approaches are taken to describe the humidity structure of the entrainment zone. The first approach models the frequency distributions of the three types of air in the entrainment zone: unmixed free atmosphere (dry); unmixed surface layer air (moist); and a mixture of these two. The resultant modeled frequency distributions of specific humidity capture the following observed features: Low in the convective boundary layer, surface layer air is frequently observed with little mixture air and no free atmosphere air. Higher in the convective boundary layer, near the middle of the entrainment zone, the proportion of unmixed free atmosphere and mixture air increases while the proportion of unmixed surface layer air decreases. Approaching the top of the entrainment zone, unmixed surface layer and mixture air proportions decrease to zero leaving only unmixed free atmosphere air. These results are critical for the successful forecasts of fair-weather cumulus. The second approach uses the linear mixing character of air with different specific humidities and yields vertical profiles of the proportion of surface layer air present. These profiles are described well by the cumulative distribution function of asymmetric double exponential functions.

1. Introduction

The turbulent interface between the stable capping layer aloft and the convective boundary layer (CBL) or mixed layer (ML) below is called the entrainment zone (Deardorff et al., 1980), a region of finite depth that is roughly 10% to 40% of the depth of the ML. Most of the interaction/mixing between the mixed layer and free atmosphere takes place in the entrainment zone. Through the entrainment processes taking place here, warmer air is entrained into the mixed layer from the stable capping layer (Ball, 1960), and drier and often less polluted air from aloft is entrained in this region to add to the mixed layer's depth and change the physical properties and composition of the mixed layer.

Figure 1 shows an example of how the daytime CBL and location of the entrainment zone appear on a lidar range–height indicator (RHI) scan (X–Z plane). The heights indicated in Fig. 1 are subjectively determined using the following definitions:

(i) The top of the highest thermal defines h_2, the top of the entrainment zone.

(ii) The average mixed layer depth is defined as Z_i, where a 50–50% mixture of mixed layer air from below and free atmosphere air from above exists.

(iii) The bottom of the entrainment zone, h_0, is where 90%–95% of the air is mixed layer air.

A sequence of lidar RHI scans can be subjectively analyzed to follow the evolution of the daytime CBL and to resolve the depth of the entrainment zone. Figure 2 shows an example of the daytime growth of the CBL and changes in the depth of the entrainment zone in response to solar heating of the earth's surface.

Since cumulus cloud cover fraction is dependent on the amount of CBL air that reaches and exceeds its lifting condensation level (LCL), precise measurement of the amount of CBL air as a function of height in the entrainment zone is required. Wilde et al. (1985) demonstrate that there is a natural horizontal variability of the LCL from thermal to thermal and that the expected coverage of cumulus clouds is related to the probability that CBL air is likely to be at or above its local LCL. Unfortunately, Wilde et al. (1985) lacked accurate information on the frequency distribution of the CBL air in the atmospheric entrainment zone. Manton's (1982) research confirmed that knowledge of the average CBL height without entrainment zone information is insufficient for determining cumulus onset and coverage. Thus, the present study is moti-

* Present affiliation: Headquarters, Air Force Global Weather Central, Offutt AFB, NE 68113-5000.

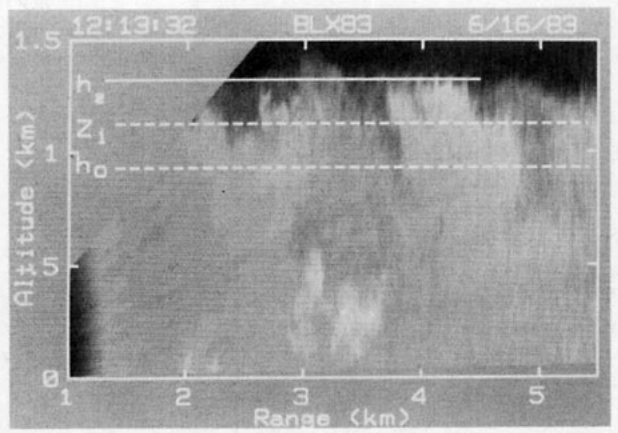

FIG. 1. Lidar range height indicator scan at 1213 CDT 16 June 1983. Thermals in the mixed layer appear white or gray, while capping stable layer air from the free atmosphere appears black in this computer enhancement. The average CBL height (Z_i) is indicated on the image as well as the bottom (h_0) and top (h_2) of the entrainment zone. The depth of the entrainment zone is $h_2 - h_0$. The heights h_2, Z_i, and h_0 are subjectively determined.

vated by a real need for detailed measurements of entrainment zone structure.

Despite the importance of the entrainment zone in understanding the growth of the CBL and the onset of cumulus clouds, little observational data exist on the entrainment zone characteristics (Caughey et al., 1979; Palmer et al., 1979). Some ground-based and airborne lidar measurements of entrainment zone thickness were obtained by Boers et al. (1984) and Melfi et al. (1985). The scarcity of observations is due in part to the relative inaccessibility of the entrainment zone to direct measurements.

Deardorff et al. (1980) simulated the atmospheric CBL and entrainment zone in a water-filled laboratory tank. Using milk as a tracer of the simulated CBL (versus clear water for the stable layer above) Deardorff et al. obtained estimates of the amount of CBL fluid reaching various levels in the tank by illuminating thin horizontal layers of the tank with a spread laser beam and then photographing the tank from above. The resultant vertical profile of the amount of CBL air reaching given altitudes smoothly varies from 90% at the bottom of the entrainment zone to 0% at the top, and has a shape resembling the cumulative distribution function of a double exponential function (Wilde et al., 1985). This profile contrasts with one approximated by a power law used by Manton (1982) in a fair-weather cumulus model. Manton estimated the exponent in his power law after looking at the results of earlier laboratory tank experiments by Deardorff et al. (1969), but states that the choice was somewhat arbitrary and needs to be tested explicitly.

This paper outlines the methodology (section 2) and results (section 3) from an analysis of field experiment data to determine the humidity structure of continental atmospheric entrainment zones. One of the major analyses (section 4) concerns the original sources for air that move into the entrainment zone and the resulting mixtures and relative concentrations. These results are applicable to cloud formation and cloud-cover studies, because one of the diagnosed quantities is the amount of undiluted high-humidity air from the surface layer. The second major analysis (section 5) concerns the total transport of surface layer air into the entrainment zone regardless of dilution. This result is potentially applicable to pollution transport to the region of the cloud-topped boundary layer where aqueous-phase reactions require knowledge of pollutant input flux and concentrations.

2. Methodology

a. Field experiment and data reduction procedures

The dataset for this study was collected during May and June 1983 at a site 60 km southwest of Oklahoma City, Oklahoma during Boundary Layer Experiment 1983 (BLX83) (Stull and Eloranta, 1984). The primary data sources for this paper were fast-response Queen Air aircraft sensors and the University of Wisconsin ground-based lidar (Sroga et al., 1980; Kunkel et al., 1977).

During the field experiment, the lidar observations of Z_i were used to direct the aircraft flight patterns and altitudes. The resulting aircraft data were then normalized with respect to the lidar-observed entrainment zone and mixed layer depth.

The Queen Air flew a sequence of straight and level flight legs in a race track pattern with one side of the pattern (18 to 30 km long) aligned with the lidar's center beam (see Fig. 1 of Stull and Eloranta, 1984). On days with no clouds, these legs were flown at preplanned altitudes relative to Z_i in order to collect data in the

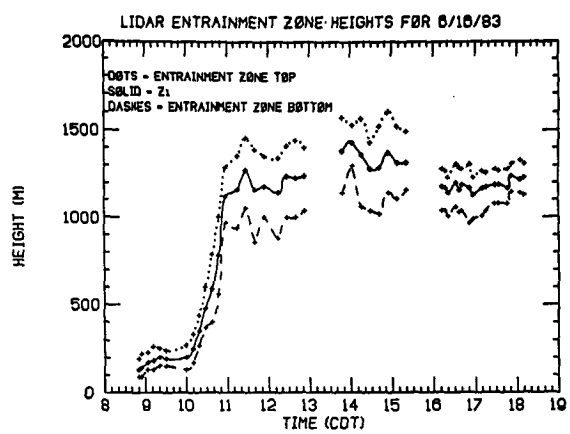

FIG. 2. Daytime change of entrainment zone depth as subjectively determined from lidar RHI imagery for 16 June 1983. Missing heights are due to lidar equipment outages. The lower heights after 1530 CDT are due to the effects of subsidence.

entrainment zone. The sequence of horizontal flight legs, preceded and followed by an ascending or descending sounding leg made from near the surface to above the top of the entrainment zone, was known as an "entrainment zone flight." Also, low altitude (20 to 40 m AGL) horizontal flight legs were flown immediately preceding or following the soundings so that an estimate of the surface layer conditions and fluxes could be obtained.

The Queen Air data for each horizontal flight leg were linearly detrended, despiked such that observations more than five standard deviations from the leg average were replaced with the previous value and filtered so that the contributions of mesoscale variations with wavelengths greater than 6.25 km were removed. The 20 Hz Lyman alpha output voltages were converted to meteorological units of humidity. The 20 Hz sample rate combined with the aircraft speed allows a horizontal resolution of approximately 4 m. Information concerning the Queen Air sensors and the data collection system can be found in NCAR *RAF Bulletin No. 2* (1981), Lenschow et al. (1978) and Duncan and Brown (1978).

The dataset used for these case studies was collected by the Queen Air on three cloud-free days (28 May, 14 June and 16 June 1983), during which five full sequences (i.e., five cases) of entrainment zone flight legs were flown. Only one representative set of flight legs will be shown and discussed in detail in this paper. On these days the field site was experiencing anticyclonic conditions with relatively weak gradients and weak advection of temperature and humidity.

b. Analysis procedure

Analysis of observations of the CBL made by the lidar and the Queen Air confirm that specific humidity can be used as a discriminator between air originating in the free atmosphere (FA) and air originating in the surface layer (SL). It is suggested that the specific humidity observed at each point in a horizontal flight leg describes one measure of the origin of air at that point. Crum et al. (1987) describe in greater detail the coincident lidar and Queen Air analysis leading to this conditional sampling criteria.

The work in this paper relies on the use of frequency distributions of specific humidity to make statements on entrainment zone structure and physics. In applying this concept, we assume that:

1) The 18–30 km long flight legs provide adequate samples of the entrainment zone in the field-experiment region, and the line samples are representative of a horizontal (X–Y plane) area.

2) The CBL was quasi-stationary during the 30-minute to one-hour period that any one entrainment zone pattern was flown.

3) The highest flight leg, which was flown at an altitude just above the tops of the highest thermals detected by the lidar, is representative of free atmosphere (FA) conditions. Similarly, the lowest flight leg, which was flown at an average relative altitude of $Z/Z_i = 0.02$, is representative of surface layer (SL) conditions.

3. Analysis results of sources and mixtures

Horizontal flight leg data were analyzed to determine the frequency of occurrence of various specific humidities at each flight altitude. Parcels from the FA are relatively dry, while parcels originating near the surface are more moist. For example, the histogram of specific humidities observed during a horizontal flight leg at $1.01Z/Z_i$ (Fig. 3) shows a trimodal distribution of humidities, suggesting the presence of 1) unmixed surface layer (SL) air; 2) unmixed free atmosphere (FA) air; and 3) air resulting from a mixture of air from the first two source regions. This trimodal distribution is typical of histograms of specific humidity collected near $1.0Z_i$. The tendency for the mixed air to have an expected value/mode between those of the two source regions will be discussed in section 5.

Histograms similar to Fig. 3 were prepared for consecutive flight legs at other altitudes, thereby creating a more complete picture of mixing as a function of height. An example of a composite set of histograms is presented in Fig. 4 in an arrangement showing where the histograms were obtained relative to the features at the corresponding specific humidity sounding. The histogram corresponding to the highest flight leg (leg 4) shows the frequency distribution of specific humidity for nearby unmixed FA air. Similarly, the lowest flight leg (leg 11) histogram gives the distribution for unmixed SL air. By using these two histograms as "reference"

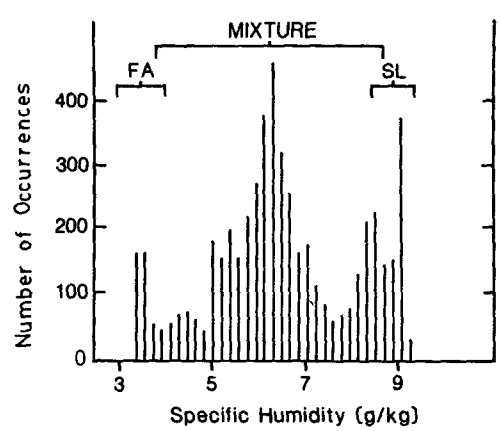

FIG. 3. Histogram of relative frequency of occurrence of specific humidity measured by the Queen Air during a horizontal flight leg. The leg was flown at $1.01Z/Z_i$ between 1145 and 1149 CDT 16 June 1983. The general character of the three types of air existing in the entrainment zone are evident here: 1) unmixed free atmosphere (FA) air centered at 3.4 g kg^{-1}; 2) unmixed surface layer (SL) air centered at 8.5 g kg^{-1}; and 3) mixture air centered at 6.3 g kg^{-1}.

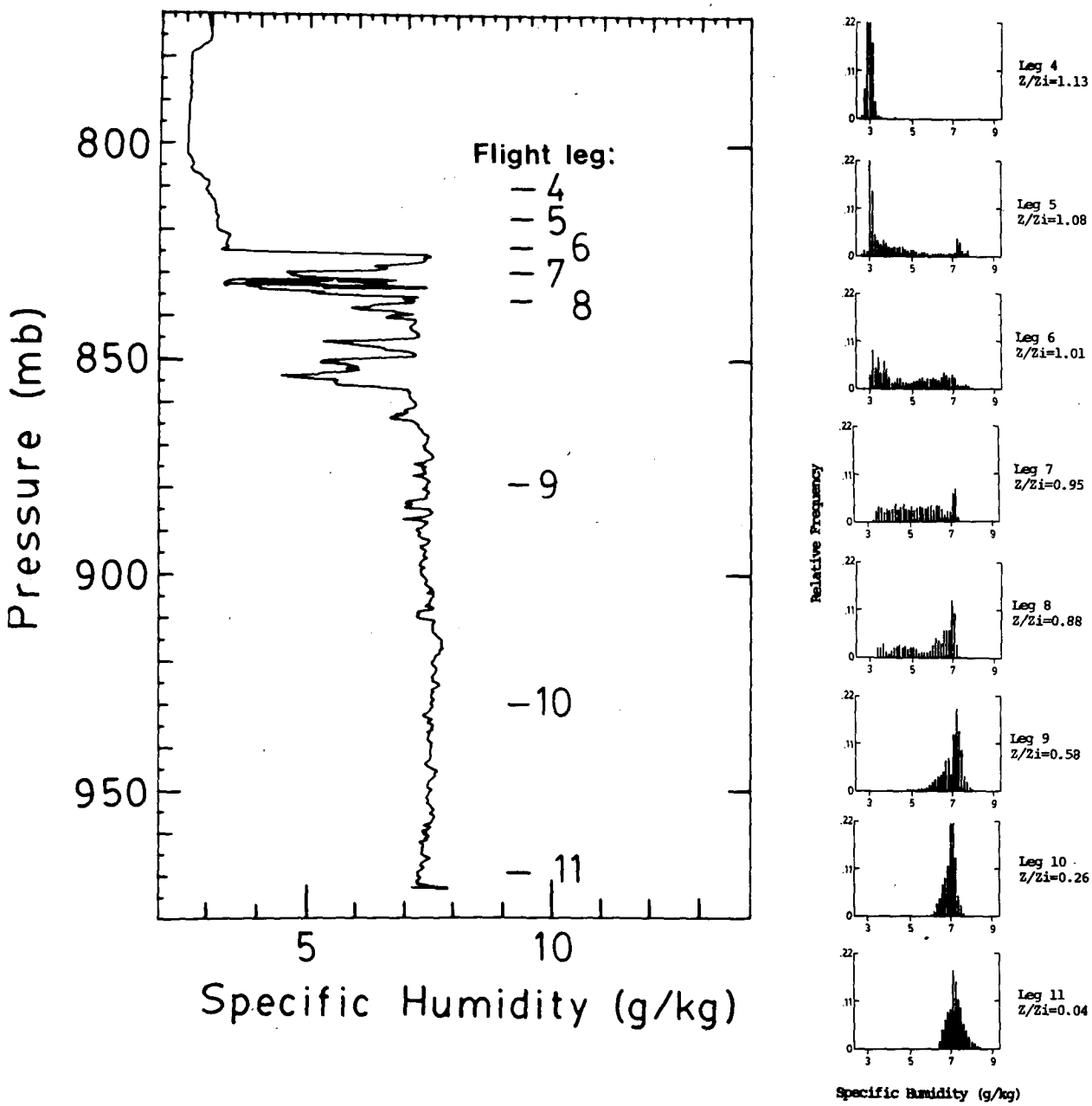

FIG. 4. Vertical profile of specific humidity from Queen Air sounding showing altitudes where various horizontal flight legs (4–11 in this case) were flown. Histograms (relative frequency of occurrence) of specific humidity values measured during horizontal flight legs 4–11 of Flight 13 between 1437 and 1532 CDT 14 June 1983 are also shown. The heights of these legs are relative to the average CBL height (Z_i) estimated from lidar data. Leg 11 is the surface layer reference leg and leg 4 is the free atmosphere reference leg. For each histogram, the ordinate gives the relative frequency of occurrence and the abscissa is specific humidity in values of g/kg.

measures of two distinct air masses, one can analyze the midlevel histograms in terms of air originating from these source regions. In particular, one can estimate the fraction of unmixed FA air, unmixed SL air, and mixture air (i.e., non FA or SL air) at each height. Different unmixed FA and SL air specific humidity frequency distributions are used as references for each set of entrainment zone flight legs, because the surface and free atmosphere reference environments change with time.

Several statements and definitions can be made based on Fig. 4:

1) The shape and modal value of humidity of the FA and SL frequency distributions remain fairly constant as altitude from the respective source region in-

creases, although the amount of air with those respective frequency distributions decreases with increasing distance from the sources.

2) Values of specific humidity characteristic of those found in the FA source region are found below $1.0Z_i$, indicative of plunges of FA air down into the CBL. Unmixed FA air does not penetrate far into the EZ (in this case taken in midafternoon, after the greatest rate of growth of the CBL has taken place), although air containing a mixture of FA and SL air is found in the lower third of the CBL. The converse is not true, because unmixed near-surface specific humidity values are indeed seen at the tops of the tallest thermals.

3) The shape of the humidity frequency distributions for both SL and FA air is somewhat variable from flight to flight. Nevertheless, the distributions for air from these two source regions can usually be approximated by an asymmetric double exponential density function.

4) Intermediate specific humidity values (between those of the SL and FA) also exist in the EZ. The frequency distribution of these humidities is associated with what will be called "mixture air." The distribution of mixture air can be approximated by a Gaussian distribution function.

5) The vertical variation of overall frequency distribution of specific humidity involves a general change in the relative proportions of SL, FA, and mixture air. The observed humidities near the top of the EZ consist mostly of FA air while the proportion of FA air decreases at lower altitudes. At intermediate levels, there are more frequent occurrences of mixture air, and the mode of this mixture shifts towards greater humidities as one descends. At some levels, the mode of mixture air is nearly adjacent to that of the FA or SL air, and no "gaps" between the FA or SL air frequency distributions are apparent.

The amount of mixture air at a level in the EZ is primarily a function of large-scale eddy mixing. Because of shear and the sinking of overshooting thermals, large volumes of FA air, mixture air, and SL air are intermixed. Only a small amount of air is mixed along the side of thermals via smaller-eddy lateral entrainment. One of the results of the work reported in Crum et al. (1987) was the realization that lateral entrainment does not proceed far into thermals. Most of the lateral entrainment is limited to a narrow region next to the edges (typically less than 15% of the diameter of active thermals) termed the "intromission zone." The presence of these relatively undiluted thermal cores helps to explain the occurrence of some unmixed SL-origin air near the top of the EZ.

Deardorff et al. (1980) visually estimated the fraction of mixed layer (ML) fluid existing at a given height in the EZ in their laboratory tank simulation with a stated 10% accuracy. Since they had only two categories (SL and FA), they classified mixtures with any SL fluid present as SL fluid. With our dataset, we can discriminate mixture air from SL air, which is critical for cloud forecasting because there are many situations where clouds will form in air of SL origin (high humidities) well before they can form in mixture air (lower humidities).

In the following stochastic parameterization, the three categories of air will be kept distinct. An alternative analysis and parameterization is presented in section 5 to obtain an estimate of the amount of near-surface layer air that exists in the entrainment zone regardless of dilution.

4. Source and mixture parameterization

a. Statistical approach

Lidar imagery and the histograms of specific humidity as a function of height (Fig. 4) suggested three basic populations of air parcels existing in the EZ: 1) unmixed free atmosphere (FA) air; 2) a mixture of SL and FA air; and 3) unmixed surface layer (SL) air. Each population has its own characteristic frequency distribution shape. It is hypothesized that the frequency distributions of unmixed FA air and unmixed SL air can be approximated by asymmetric double exponential probability density functions. The analytical form of the asymmetric double exponential is given by

$$f(q) = \begin{cases} A \exp[-(q - q_m)/\alpha] & q_m \leq q < q_T \\ A \exp[(q - q_m)/\beta] & q_B \leq q < q_m \end{cases} \quad (1)$$

where q_B and q_T are the smallest and largest (respectively) observed values of specific humidity in the frequency distribution, A is a normalization factor, q_m is the point of asymmetry (i.e., the mode), and α and β are shape parameters.

The shape parameters (α and β) of the asymmetric double exponential densities for the FA and SL air can be analytically found via the method of maximum likelihood estimation (MLE). The MLE estimators were selected rather than estimates from a graphical technique or method of moments because MLE parameter estimates of density functions often are the minimum variance unbiased and most consistent estimators available. Figure 5 shows an example of the resultant fit for both SL and FA legs.

Because the mixture air is the result of an indeterminate number of mixing interactions, we hypothesize that the distribution of the mixture air can be approximated with Gaussian distributions. That is, the limit of many interactions/convolutions of various probability distributions of random variables (air parcels interacting) is a Gaussian distribution. The form of the Gaussian distribution is

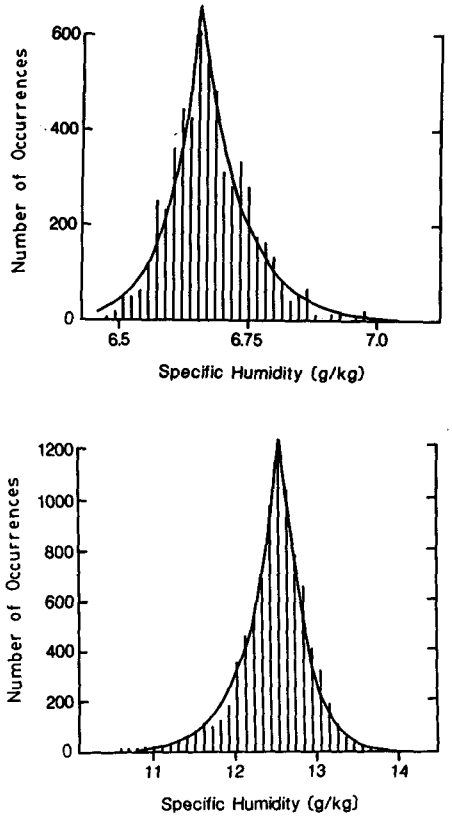

FIG. 5. Example fits of asymmetric double exponential function to the histogram of 20 Hz specific humidities observed by the Queen Air during (a) a free atmosphere flight leg and (b) a near-surface flight leg. Estimates of the parameters of the asymmetric double exponential were determined by the observations via the method of maximum likelihood.

$$f(q) = \frac{1}{\sigma\sqrt{2\pi}} \exp\left[\frac{-(q-\mu)^2}{2\sigma^2}\right] \tag{2}$$

with mean μ and standard deviation σ.

Figure 6 shows an example of how the hypothesized three density functions in the EZ sum to yield an overall distribution. Examination of the distributions in Fig. 4 suggest that this type of interaction is taking place between the FA and SL air. The overall frequency distribution of specific humidity (q) at a level in the CBL can be described by a sum of the individual population distributions weighted by their relative proportions, P_i,

$$f(q; P_i, \mu, \sigma) = \sum_{i=1}^{3} P_i g_i(q; \mu, \sigma) \tag{3}$$

where g_1 is the functional form of the unmixed FA air frequency distribution [of the form of (1)], assumed to be double exponential and known; g_2 is the form of the mixture air frequency distribution, assumed to be Gaussian [of the form of (2)] with unknown μ and σ; and g_3 is the form of the unmixed SL air frequency distribution [of the form of (1)], assumed to be double exponential and known. The mean of each function is μ and its standard deviation is σ. The sum of the unknown proportions ($P_1 + P_2 + P_3$) is unity.

In solving for the unknowns in (3) by the method of maximum likelihood, we allowed the location parameters q_1 and q_3 for the double exponential distributions to shift slightly to account for horizontal nonhomogeneity and for temporal changes of the specific humidity in the surface layer. Analysis showed that with consecutive (in time) flight legs at the same altitude, the frequency distributions of specific humidity would generally look similar but their absolute location might shift.

The logarithim of the likelihood function for (3) is

$$L = \sum_{i=1}^{N} \ln[P_1 g_1(q_i; q_{m1}, \alpha_1, \beta_1) + P_2 g_2(q_i; \mu_2, \sigma_2) + P_3 g_3(q_i; q_{m3}, \alpha_3, \beta_3)] \tag{4}$$

where N is the number of observations during the flight leg. The desired values of the unknown parameters (q_{m1}, q_{m3}, P_1, P_3, μ_2 and σ_2) are the values which maximize this function. This procedure was performed separately for each flight leg.

The result of this effort will be estimates of the proportion of the three types of air and parameters of the assumed Gaussian distribution of the mixture air existing at various flight levels. In addition to being able to discover what these values are, these parameters provide the information needed to describe the theoretical distribution of specific humidities at any level in the entrainment zone.

b. *Estimates of source and mixture proportions*

The modeled frequency distributions of specific humidity to be found are essentially the result of fitting the hypothesized frequency distributions (Fig. 6) to the observed frequency distribution (e.g., Fig. 3). Table 1 lists the maximum likelihood estimates of the proportions of the three types of air present in the CBL for the entrainment zone flight legs flown during BLX83.

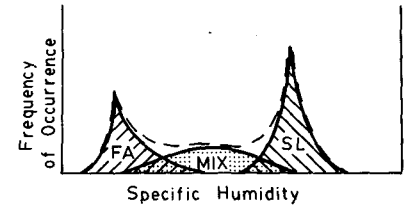

FIG. 6. Graphic example of how three density functions (FA, unmixed free atmosphere air; MIX, air which is a mixture of various proportions of FA and SL air; and SL, unmixed surface layer air) sum to produce the observed density function (dashed line).

TABLE 1. MLE estimates of the parameters in (4), giving the proportions of the sources and mixtures (to the nearest 0.01). These parameter estimates were obtained by numerically evaluating (4) for the maximum value obtained. See Table 2 for start times and altitude of each leg.

Leg	Z/Z_i	Proportions FA	MIX	SL	μ_2 (g kg^{-1})	σ_2 (g kg^{-1})
Flight 3, 28 May 1983						
Case A						
4	0.31	0.0	0.0	1.0	11.70	0.77
5	0.65	0.0	0.05	0.95	10.92	0.59
6	0.87	0.0	0.39	0.60	10.92	1.11
7	0.93	0.0	0.6	0.4	10.4	1.31
8	1.02	0.09	0.77	0.14	8.39	1.48
9	1.13	0.8	0.14	0.06	8.01	1.34
Case B						
15	0.38	0.0	0.0	1.0	10.03	1.92
16	0.83	0.0	0.43	0.57	11.75	0.7
17	0.99	0.02	0.5	0.47	10.31	1.53
19	1.27	0.3	0.64	0.06	5.79	1.51
Flight 13, 14 June 1983						
Case C						
5	1.08	0.55	0.33	0.12	4.26	0.76
6	1.01	0.2	0.66	0.15	4.9	1.21
7	0.95	0.08	0.7	0.21	5.21	0.87
8	0.88	0.07	0.36	0.57	4.93	0.75
9	0.58	0.0	0.26	0.74	6.5	0.66
10	0.26	0.0	0.0	1.0	6.5	0.76
Case D						
17	0.94	0.0	0.78	0.22	5.87	0.75
18	0.89	0.0	0.5	0.5	6.55	0.44
19	0.66	0.0	0.11	0.89	6.77	0.11
20	0.32	0.0	0.0	1.0	7.05	0.17
Flight 16, 16 June 1983						
Case E						
6	1.01	0.07	0.71	0.21	6.20	0.96
7	0.93	0.0	0.66	0.34	7.79	0.93
8	0.83	0.0	0.53	0.47	8.21	0.49
9	0.62	0.0	0.3	0.7	8.27	0.41
10	0.41	0.0	0.11	0.89	8.33	0.24
11	0.21	0.0	0.0	1.0	8.24	0.64

Figure 7 graphically depicts the vertical profiles of these MLE parameter estimates for one set of flight legs.

Quantitatively the estimates of the mean and standard deviation of the mixture air follow the patterns expected. Mixture air parcels near the bottom of the EZ have relatively large values of mean humidity, because they have probably experienced more interactions with other mixture parcels and SL parcels (due to the closeness of the SL source region) than they would have aloft. Also, at the bottom of the EZ, many mixings have tended to reduce the range of specific humidity found in mixture air. Near the center of the entrainment zone, there are plunges of FA air just beginning to mix, unmixed and nearly unmixed SL air in active thermals and in neutrally buoyant thermals, and mixture air from earlier mixings which all have a long period of time to interact. This sets up a large range of mixture air specific humidities and largest standard deviation of specific humidity near Z_i. As one goes higher in the entrainment zone, the expected (mean) value of mixture air specific humidity decreases. Lidar imagery suggests this too. Near the top of the EZ, fewer scales of turbulent mixing are in action and the parcels of SL air/thermals at this level are there for a very short period of time. Hence, a narrower range of specific humidity values result.

The qualitative ramifications are that the mean humidity (and hence location on the frequency distribution) shifts from high to low humidity as one makes measurements from the bottom to the top of the entrainment zone. Also, the amount of mixture air dominates near the middle of the EZ, while FA and SL air dominate near the top and bottom of the EZ, respectively.

One check on the goodness of the hypothesis that the entrainment zone air consists of only three populations with the specified frequency distributions is to compare the observed and modeled/fitted frequency distributions of specific humidity. The modeled distribution (Fig. 8) captures the major features seen in the observed distribution (Fig. 4).

The approach used above provides the vertical profile of the proportions of the three types of air present in the EZ and parameters of the probability distributions.

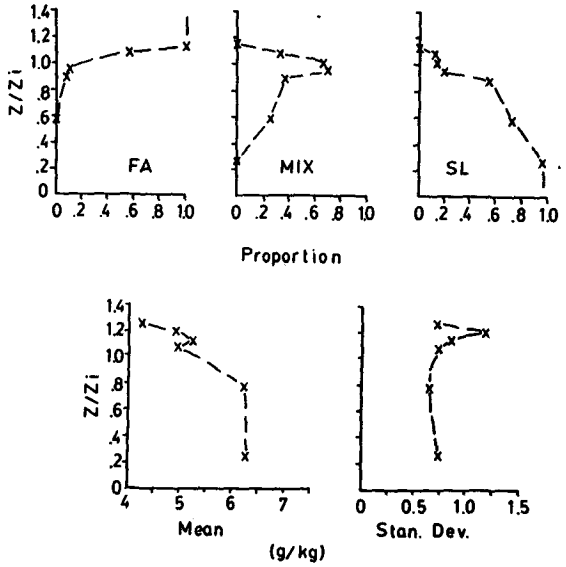

FIG. 7. Vertical profiles of source and mixture proportions and distribution parameters for Flight 13 legs 4–10, 14 June 1983. The heights have been normalized by the mean CBL height (Z_i). The top row of graphs show the estimates of the proportion of the three types of air existing in the entrainment zone (FA, unmixed free atmosphere air; MIX, a mixture of free atmosphere and surface layer air; and SL, unmixed surface layer air). The sum of these proportions equals one at each height. The bottom two graphs show the estimates of the mean and standard deviation of the hypothesized Gaussian distribution of the mixture air frequency distribution. See text for details on the parameter estimation.

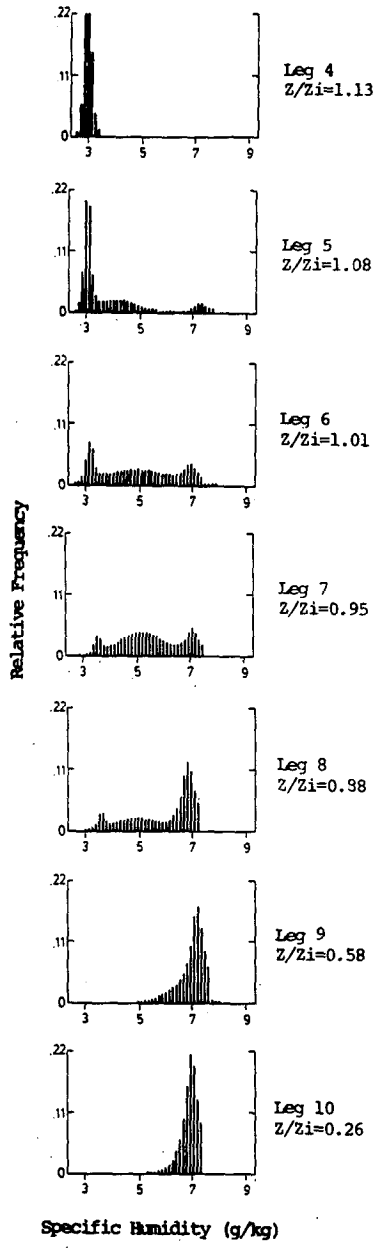

FIG. 8. Modeled frequency distributions of specific humidity for legs 4–10 of Flight 13, 14 June 1983. The modeled distribution is composed of the sum of asymmetric double exponential functions for FA and SL air while the assumed frequency distribution of the mixed air is Gaussian. The observed distributions are shown in Fig. 4. The Y axis is relative frequency of occurrence and the X axis is specific humidity (both held constant on this figure) in g/kg.

Knowledge of these values allows construction of the hypothesized specific humidity frequency distribution for any height—not just the levels where observations were made. This is particularly valuable for cloud-cover forecasts, where knowledge of the amount of undiluted surface-layer air is critical (Wilde et al., 1985). An analytical expression was sought to describe the curves from the five EZ flights as a function of CBL scaling parameters. Unfortunately the limited sample size precluded any smooth fits. Future field experiments can hopefully overcome this shortfall.

5. Transport from the surface layer

Next, we apply another sampling methodology to our dataset to obtain estimates of the total amount of SL air (whether mixed or unmixed) present in the entrainment zone. Although humidity is used as the passive tracer in this study, the results can be applied to other tracers of surface origin. This could be potentially valuable for pollution venting and aerosol swelling studies at the top of the boundary layer, where the amount of tracer transported, rather than its concentration, is most important.

a. Linear mixing technique

The resultant specific humidity of all possible ratios of mixtures of two volumes of air (not just the mixture of equal volumes) lie along a mixing line (Betts, 1982). The location of the mixture on the mixing line is determined by the proportions of air mixed.

If we assume that we know the specific humidity of the two types of air involved in the mixing (FA and SL) then we can find the fractional amount of surface layer air (F_{SL}) in the resultant mixture at any one point in space by

$$F_{SLi} = \frac{q_{OBSi} - q_{FA}}{q_{SL} - q_{FA}} \tag{5}$$

where q_{OBSi} is the specific humidity of the ith parcel sampled, q_{SL} is the minimum specific humidity observed during the representative near-surface flight leg, and q_{FA} is the maximum specific humidity observed in the free atmosphere just above the CBL. This results in the following possible values for F_{SLi}:

$$F_{SLi} = \begin{cases} 0, & q_{OBSi} < q_{FA} \\ \dfrac{q_{OBSi} - q_{FA}}{q_{SL} - q_{FA}}, & q_{FA} \leqslant q_{OBSi} \leqslant q_{SL} \\ 1, & q_{OBSi} > q_{SL}. \end{cases}$$

Using the linear mixing character of specific humidity, the fractional amount F of SL air in the EZ sampled during an entire flight leg is merely the sum of the contributions from individual sampling points along the leg:

$$F = \frac{1}{N} \sum_{i=1}^{N} F_{SLi} \tag{6}$$

where N is the number of observations during the flight leg. Here F_{SLi} is determined from (5).

b. Resultant profiles of entrainment zone structure

Table 2 contains the estimated proportion F of surface layer air at various altitudes estimated by the linear mixing approach. Figure 9 is a graphical representation of the proportions as a function of normalized height for one sequence of flight legs. The shape of this and the proportion profiles from the other four flights is well fit by the cumulative distribution function (CDF) of asymmetric double exponential functions. The appropriate CDF is drawn in as the dashed line in Fig. 9. This is similar to the profile shape that Wilde et al. (1985) reported to fit the Deardorff et al. (1980) tank data of the ML fluid in the simulated EZ.

The shape of the curve for F in Fig. 9 and Table 2 is parameterized with the CDF of the asymmetric double exponential function. This use of the asymmetric double exponential function should not be confused with its use in fitting frequency distributions in section 4. The CDF is the integral of the probability density function (PDF) of the asymmetrical double exponential, as seen in (1). Thus, the fraction F at height H is

$$F(H) = \begin{cases} A\beta\{\exp[(H - Z_m)/\beta] - \exp[(Z_B - Z_m)/\beta]\}, \\ \qquad\qquad H \leqslant Z_m \\ A\beta\{1 - \exp[(Z_B - Z_m)/\beta]\} \\ \quad + A\alpha\{1 - \exp[-(H - Z_m)/\alpha]\}, \quad H > Z_m \end{cases} \tag{7}$$

where Z_B is the height of the lowest flight leg, A is a normalization factor which allows the total area under the function to equal one, and Z_m is the point of asymmetry.

Equation (7) is then solved for the parameters (α, β, Z_m) which result in the smallest sum of squares difference between the function and the observations. The parameters of the cumulative distribution functions that best fit these entrainment zone flight profiles are listed in Table 3.

In Table 3 the inflection point of the fitted CDFs (Z_m) is consistently near the subjectively determined (from lidar imagery) mean CBL depth Z_i, suggesting that the mean CBL height might be the transition point of two mixing characteristics because the inflection point in this CDF occurs where the two exponential probability distribution functions join to form the double exponential distribution. Above Z_i the thermals are primarily interacting with the FA air for a short time and mostly in a SL–FA mixture. Below Z_i the time scale for interactions is larger. Hence, Z_i is more than just a convenient label to call the depth of the CBL.

The shape parameters α and β for these fits do not appear to be related to the most appropriate CBL parameters. Earlier entrainment zone work has suggested that the depth and character of the entrainment zone is related to: 1) the change of buoyancy across the capping stable layer $\Delta\theta_v$; 2) the buoyancy flux at the sur-

TABLE 2. Estimates of the proportion of surface layer air existing at various levels in the CBL as measured by the Queen Air and applying the linear mixing indicator function.

Leg	Start time (CDT)	Altitude (m AGL)	Z/Z_i	Proportion of SL air
		Flight 3, 28 May 1983		
Case A				
3	1501	57	0.07	1.00
4	1508	232	0.31	0.999
5	1515	467	0.65	0.994
6	1520	619	0.87	0.941
7	1527	663	0.93	0.850
8	1533	722	1.02	0.41
9	1539	800	1.13	0.094
10	1545	859	1.22	0.016
11	1552	929	1.25	0.0
Case B				
14	1625	57	0.07	1.0
15	1631	297	0.38	0.996
16	1638	619	0.83	0.979
17	1644	745	0.99	0.836
18	1650	830	1.13	0.403
19	1656	919	1.27	0.137
20	1702	1018	1.36	0.0
23	1742	94	0.13	1.0
		Flight 13, 14 June 1983		
Case C				
1	1414	65	0.03	1.0
4	1437	1621	1.13	0.0
5	1445	1549	1.08	0.209
6	1452	1488	1.01	0.452
7	1458	1427	0.95	0.636
8	1505	1356	0.88	0.756
9	1512	927	0.58	0.991
10	1519	443	0.26	1.0
11	1527	84	0.04	1.0
Case D				
14	1550	2047	1.15	0.026
15	1557	1961	1.08	0.04
16	1604	1866	1.01	0.69
17	1611	1771	0.94	0.848
18	1618	1678	0.89	0.969
19	1624	1222	0.66	0.998
20	1632	594	0.32	1.0
22	1645	66	0.02	1.0
		Flight 16, 16 June 1983		
Case E				
1	1111	58	0.05	1.0
5	1138	1438	1.12	0.0
6	1145	1306	1.01	0.589
7	1151	1176	0.93	0.905
8	1158	1078	0.83	0.977
9	1204	795	0.62	0.991
10	1212	533	0.41	0.999
11	1218	272	0.21	1.0
12	1225	61	0.05	1.0

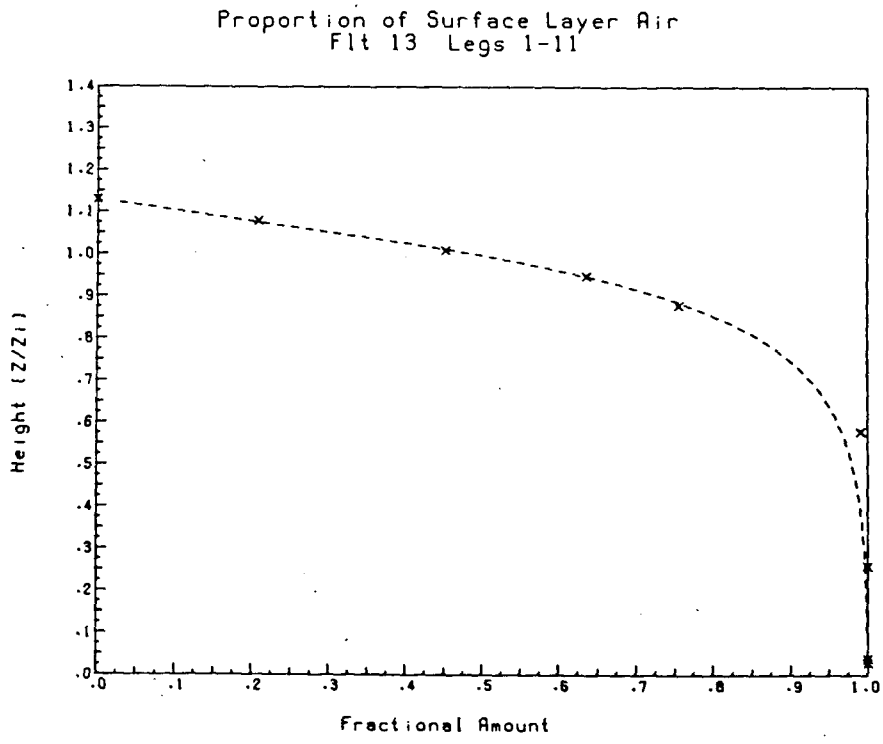

FIG. 9. Plot of proportion of surface layer air present as a function of normalized height. The estimates are from the linear mixing approach. The best fit line of a cumulative distribution function of an asymmetric double exponential function is drawn. The data was collected on legs 1–11 of Flight 13, 14 June 1983.

face; 3) the convective scaling velocity w_*; 4) the interfacial Richardson number; or 5) the depth of the entrainment zone. Attempts to correlate the shape parameters with these five CBL parameters individually and in combinations were not successful (i.e., the shape parameters do not appear to be functions of the five CBL parameters examined).

A step toward successful modeling of the entrainment zone is the confirmation that the cumulative distribution function of asymmetric double exponentials describes the SL air proportion as a function of height. The consistently good fit of the five series of flight legs, flown in early afternoon when a deep mixed layer was well established, and the laboratory tank results of Deardorff et al. (1980) further our confidence that this is the profile that the proportion of SL air assumes in daytime continental CBLs.

TABLE 3. Best fit estimates of parameters of asymmetric double exponential cumulative distribution function based on proportion estimates listed in Table 2. The estimates are from the linear mixing approach. See section 5 for an explanation of terms.

Flight	Legs	α	β	$Z_m(Z/Z_i)$
3	1–11	0.088	0.061	0.99
3	13–23	0.316	0.068	1.02
13	1–11	9.424	0.155	1.03
13	13–23	0.003	0.065	1.08
16	1–12	1.725	0.054	0.99

6. Discussion and conclusions

Examination of the vertical profiles of histograms of specific humidity collected during horizontal flight legs led to the conclusion that air in the entrainment zone is composed of three types: unmodified free atmosphere air, unmodified surface layer air, and a combination of these two (mixture air). It was hypothesized that the specific humidity frequency distribution of the mixture air would have a Gaussian distribution and that the frequency distribution of the unmixed free atmosphere and surface layer air could be fit by asymmetric double exponential functions. The application of maximum likelihood estimators to the frequency distribution of specific humidity led to estimates of the proportion of the three types of air present. Vertical profiles of these proportions show that for these cases, collected after the period of greatest growth of the CBL, unmixed free atmosphere air rarely penetrates far below the mean CBL depth, and the proportion of mixture air has a maximum near the mean CBL depth. The mean humidity of the mixture air increases with decreasing height.

Knowledge of the frequency distribution of specific humidity/pressure of the lifting condensation level coupled with forecasts of Z_i can lead to more accurate cumulus forecasts. Cumulus form when air is lifted above its lifting condensation level. The above frequency distributions of specific humidity reveal variability in the humidity content of thermals. Hence, estimates of the frequency distribution of specific humidity/pressure of lifting condensation level coupled with forecasts of the depth of the CBL reduce the cumulus onset and coverage forecast problem to determining the frequency of occurrence of specific humidity/pressure of the lifting condensation level from the frequency distribution.

Using the linear mixing character of specific humidity as another approach, the profile of the proportion of surface layer air regardless of dilution that existed in the entrainment zone was found. This profile was well fit by the cumulative distribution function of asymmetric double exponential functions though the parameters of the functions do not appear to be functions of the CBL parameters. A similar profile was reported for earlier laboratory tank experiments.

Additional entrainment zone field experiments utilizing similar basic instrumentation and operations plan as was used in BLX83 should be carried out. Studies in both forced and free convection cases are suggested in order to be able to improve knowledge of the entrainment zone structure in both regimes. Also, further efforts should be made to parameterize the vertical profiles of the proportion of SL air and the three types of air present in the entrainment zone as a function of typical CBL parameters. Lastly, comparative cumulus cloud cover forecasts using previously used assumptions of the distribution of humidity in the entrainment zone and the distributions described in this study should be undertaken. The sensitivity of the forecast to the shape parameters of the double exponential cumulative distribution function should also be examined.

Acknowledgments. The first author was supported by the Air Force Institute of Technology Civilian Institutions Program during his graduate research at the University of Wisconsin. The aircraft data came from the Queen Air (N306D) operated by the National Center for Atmospheric Research (NCAR), which is sponsored by the National Science Foundation. This research was supported by NSF grants ATM-8414371 and ATM-8211842. The lidar was designed and built by Dr. Edwin Eloranta.

REFERENCES

Ball, F. K., 1960: Control of inversion height by surface heating. *Quart. J. Roy. Meteor. Soc.*, **86,** 483–494.

Betts, A. K., 1982: Saturation point analysis of moist convective overturning. *J. Atmos. Sci.*, **39,** 1484–1505.

Boers, R., R. L. Coulter and E. W. Eloranta, 1984: Lidar observations of mixed layer dynamics: Tests of parameterized entrainment models of mixed layer growth rate. *J. Climate Appl. Meteor.*, **23,** 247–266.

Caughey, S. J., and S. G. Palmer, 1979: Some aspects of turbulence structure through the depths of the convective boundary layer. *Quart. J. Roy. Meteor. Soc.*, **105,** 811–827.

Crum, T. D., R. B. Stull and E. W. Eloranta, 1987: Coincident lidar and aircraft observations of entrainment into thermals and mixed layers. *J. Climate Appl. Meteor.*, **26,** 774–778.

Deardorff, J. W., G. E. Willis and D. K. Lilly, 1969: Laboratory investigation of nonsteady penetrative convection. *J. Fluid Mech.*, **35,** 7–31.

——, —— and B. H. Stockton, 1980: Laboratory studies of the entrainment zone of a convectively mixed layer. *J. Fluid Mech.*, **100,** 41–64.

Duncan, M. T., and R. C. Brown, 1978: A data acquisition system for airborne meteorological research. *Bull. Amer. Meteor. Soc.*, **59,** 1128–1134.

Kunkel, K. E., E. W. Eloranta and S. T. Shipley, 1977: Lidar observations of the convective boundary layer. *J. Appl. Meteor.*, **16,** 1306–1311.

Lenshow, D. L., C. A. Cullian, R. B. Friesen and E. N. Brown, 1978: The status of air motion measurements on NCAR aircraft. *Preprints, Fourth Symp. Meteorological Observations and Instrumentation,* Denver, Amer. Meteor. Soc., 433–438.

Manton, M. J., 1982: A model of fair weather cumulus convection. *Bound.-Layer Meteor.*, **22,** 91–107.

Melfi, S. H., J. D. Spinhirne, S. H. Chou and S. P. Palm, 1985: Lidar observations of vertically organized convection in the planetary boundary layer over the ocean. *J. Climate Appl. Meteor.*, **24,** 806–821.

NCAR, 1981: Queen Air overview and summary of capabilities. *Research Aviation Facility Bulletin No. 2,* 10 pp.

Palmer, S. G., S. J. Caughey and K. W. Whyte, 1979: An observational study of entraining convection using balloon-borne turbulence probes and high-power Doppler radar. *Bound.-Layer Meteor.*, **16,** 261–278.

Sroga, J. T., E. W. Eloranta and T. Barber, 1980: Lidar measurements of wind profiles in the boundary layer. *J. Appl. Meteor.*, **19,** 598–605.

Stull, R. B., and E. W. Eloranta, 1984: Boundary Layer Experiment 1983. *Bull. Amer. Meteor. Soc.*, **65,** 450–456.

Wilde, N. P., R. B. Stull and E. W. Eloranta, 1985: The LCL zone and cumulus onset. *J. Climate Appl. Meteor.*, **24,** 640–657.